SENSOR-BASED ONLINE PATH PLANNING FOR ROTORCRAFT LANDING

M. Zimmermann
DLR, Institute of Flight Systems,
Lilienthalplatz 7, 38108 Braunschweig, Germany

Abstract

This paper describes a reactive path planning strategy to avoid obstacles in partially known environments during the approach-to-landing phase of a manned helicopter. As experimental platform, the research rotorcraft Active Control Technology/Flying Helicopter Simulator (ACT/FHS) is used. This highly modified EC135 is equipped with a commercial forward-looking Light Detection and Ranging (LiDAR) sensor with a range of 1 km. During an approach to an unmapped landing site, geo-referenced LiDAR samples are acquired and combined with database information. The resulting representation of the environment is used for the generation of flight paths which are collision free, technically feasible and acceptable for pilots. Once new samples are collected by the LiDAR sensor, the environment map is updated in real time and the flight path is changed based on typical approach procedures if necessary. Due to experimental aspects, a manual trajectory following was used by providing the pilot with a "Tunnel-In-The-Sky" head down display including visual cues for spatial and speed guidance during the approach. Results show the applicability of the presented planning strategy based on five approaches made to Braunschweig airport in a flight trail conducted in 2015. Furthermore, the need for proper Human-Machine-Interface design is indicated in order to communicate decisions made by the system to the pilot, which exceeds the scope of this work.

ACRONYMS

ACT/FHS	Advanced Control Technology/ Flying Helicopter Simulator
AGL	Above Ground Level
AVES	Air Vehicle Simulator
DEM	Digital Elevation Model
DSM	Digital Surface Model
DTED	Digital Terrain Elevation Data
DVE	Degraded Visual Environments
EP	Evaluation Pilot
FTE	Flight Test Engineer
IMC	Instrument Meteorological Conditions
FOV	Field of View
F3S	Flexible Sensor Simulation Suite
HMI	Human Machine Interface
LiDAR	Light Detection and Ranging
MSL	Mean Sea Level
SCC	Sensor-Co-Computer

SYMBOLS

VH	Visibility Hull
χ,γ	Flight path angles

INDICES

Hvr	Hover
Mid	Mid point of 3-point path
Start	Start point of planning
b,	base
s	safe

1. INTRODUCTION

Landing on unprepared sites is a typical mission task in day-to-day helicopter operations, which may induce high workload on pilots. As soon as the outside visual cues deteriorate, the overall workload on the pilot and the probability of a potential loss of situational awareness increases significantly. Such situations are likely to occur during inadvertent entry into instrument meteorological conditions (IMC) in higher altitudes or when particles like dust, snow or water spray are whirled up by the rotor's downwash close to the ground.

In order to enhance mission safety under IMC, the swiss helicopter emergency medical service (HEMS) provider REGA established a satellite-based Low-Flight-Network (LFN) route network for flight under instrument flight rules (IFR) in 2015 [1]. However, obstacles in the vicinity of a previously unknown mission destination may still pose threats to the

helicopter and its crew.

A study of the European Helicopter Safety Team (EHEST) shows that 28% of 487 analyzed accidents from 2005-2010 occurred in either the approach or the landing phase [2]. Very similar statistics can be found in a study of the U.S. Joint Helicopter Safety Analysis Team in Ref. [3], stating that out of 523 analyzed accidents in the years 2000, 2001 and 2006, 7% (36) occurred during approach and 21% (108) during the landing phase.

Four typical procedures for reconnaissance of a landing site can be found in a training leaflet of the EHEST in Ref. [4], summarized in Figure 1. The pilot's viewing direction is drawn as brighter arrows along the flight path. The air mass is assumed to move from right to left in these illustrations, leading to final approaches with headwind. Note that the landing site is recommended to be on the pilot's side during the orbital and flyby patterns to allow best visibility of the site. In the order of recommendations, the orbital type comes first, followed by the flyby and hover types. The last type is recommended for experienced pilots, who already know the site and can gather up-to-date visual information during a long final approach.

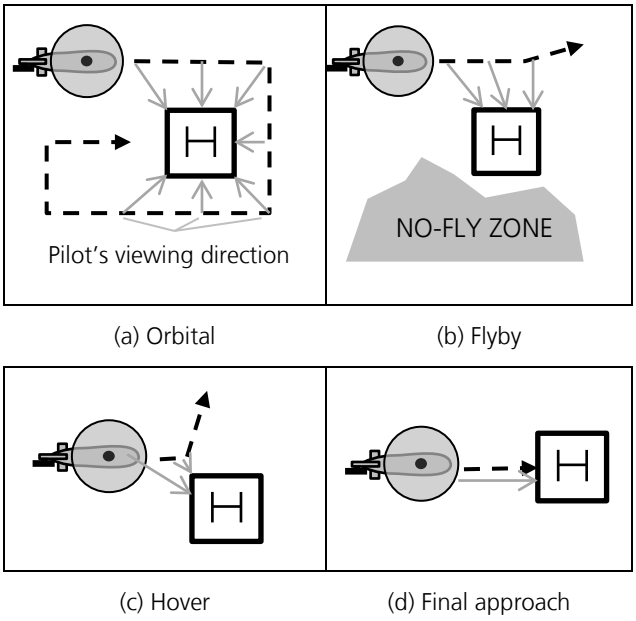

Figure 1: Four different types of landing site reconnaissance, based on Ref. [4]

Once the pilot has evaluated the size, shape, surrounds, slope and surface of the site, a final approach direction needs to be chosen and a decision for the type of approach has to be made, regardless of the previous reconnaissance type. Two types of approaches mentioned in Ref. [4] shall be considered here, namely the single and double angle approach seen in Figure 2. The air mass is assumed to move from right to left, leading to headwind approaches in both cases.

During the project ALLFlight, DLR's research rotorcraft Active Control Technology/Flying Helicopter Simulator (ACT/FHS), a highly modified EC135 seen in Figure 4, was equipped with a comprehensive perception system to find solutions for advanced pilot assistance [5]. The present work makes use of this system (see section 2) to assist the pilot by continuously proposing an unobstructed flight path during the final approach to an unprepared landing site at a known location.

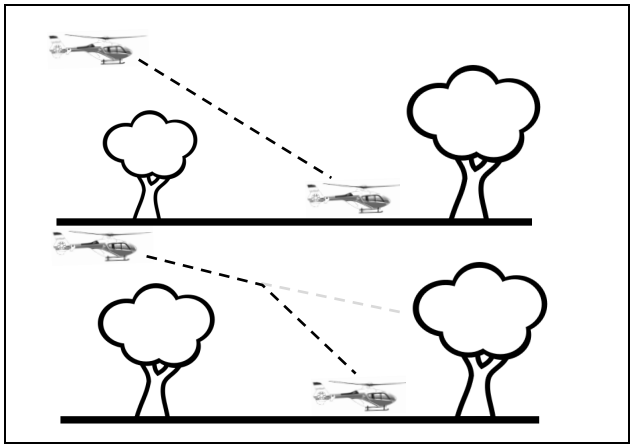

Figure 2: Single and double angle approaches

Adjacent research motivation can be found in the rotorcraft communities who are either striving for vehicle autonomy or for safer landings in degraded visual environments (DVE). Active Light Detection and Ranging (LiDAR) range sensors are common systems to gather environmental knowledge. An impressive demonstration of autonomous flight using LiDAR has been presented with the RASCAL research rotorcraft in Ref. [6] using algorithms which have been previously developed for unmanned rotorcraft (see Ref. [7]). Safe landing area determination and autonomous landing has already been demonstrated with Boeing's Unmanned Little Bird as well in Ref. [8], using a nodding line-scanning LiDAR which can scan either in flight direction or straight down. The latter mode of operation provides the possibility of a flyover-scan of the landing site, which has the benefit of almost complete terrain coverage, since no objects occlude parts of the ground. Referring to the reconnaissance types in Figure 1, this procedure can be compared to the orbital reconnaissance.

Recent research in DVE assistance in Europe and in the US presented in Refs. [9] and [10] utilizes forward-looking devices combined with "see-and-remember" systems during brown-out conditions. Guidance considering obstacles in this critical phase of flight was explicitly mentioned by pilots in the latter publication as a desired improvement, which is addressed here.

In preceding work [11] to the presented one, first flight test results of approaches using a re-planning based on geo-referenced flight surfaces and 2D-

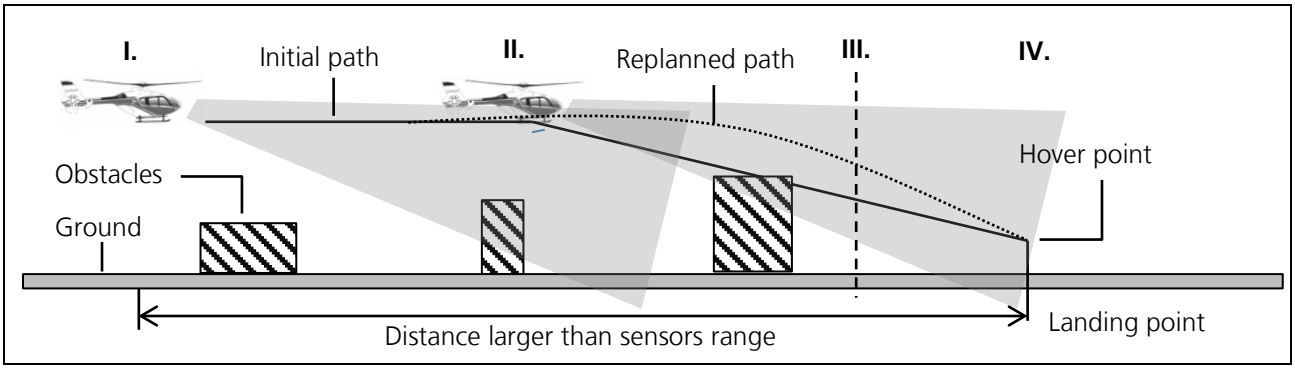

Figure 3: Intended mission scenario

visibility graphs derived from [12] was presented, using a shallow approach to Braunschweig airport as test scenario.

The body of this paper consists of three sections. The first part describes the intended mission scenario, the research vehicle and the system architecture. The second part describes the planning process and in the final part results of flight trials performed in 2015 are presented and discussed.

2. SYSTEM DESCRIPTION

The intended mission scenario is shown in Figure 3. Starting at a height above ground level (AGL) which already allows sensor coverage of the ground, an initial flight path is calculated (I.). While the pilot is following the flight path, the system is allowed to change it in case that newly detected obstacles appear in the sensor's field of view (II.). Once the helicopter is closer to the landing point than a predefined distance (III.), the flight path is kept in its last state. The pilot can finally follow the flight path until the landing point (IV.) is reached.

As experimental platform, DLR's research helicopter ACT/FHS (see Figure 4) is used. It is based on a standard EC135 but has been extensively modified for research purposes. Although equipped with a full-authority fly-by-wire/fly-by-light control system fulfilling safety requirements for civil airspace, the more relevant parts used in this work are several forward-looking sensors, described in detail in Ref. [13]. The magnified skid section in Figure 4 (upper left) shows the two passive sensors (infrared/TV camera) and a SferiSense 300 range sensor[1] [14]. Each sensor is connected to its own computing board within a cluster of seven Sensor-Co-Computers (SCC), which store, process and distribute in-flight acquired data.

The range sensor is the sole up-to-date source of environmental information in this work. Its field of view (FOV), seen in the lower part of Figure 4 is 31.5° (95 samples) in left-right and 32° (200 samples) in up-down direction, tilted by 5° downward and with a range of approximately 1 km. It delivers geo-referenced point clouds of max. 19'000 samples twice per second. Given these constraints of system perception, the starting height mentioned at the beginning of this section should be less than 250 m AGL.

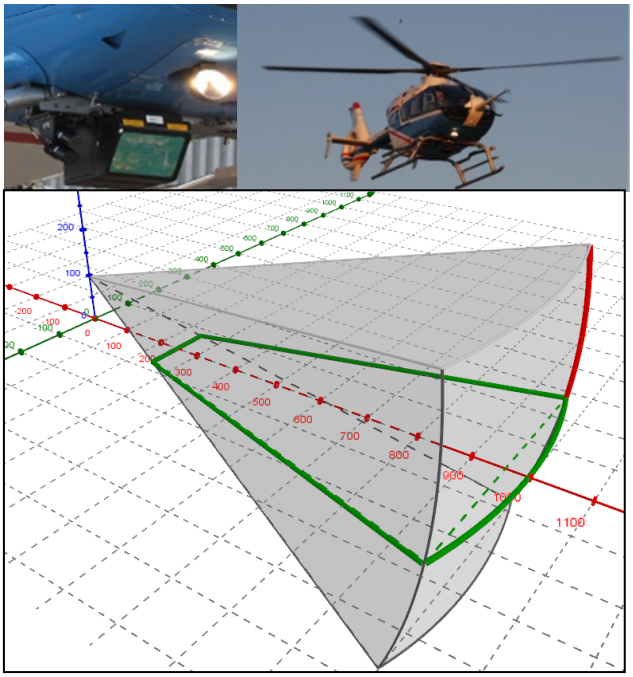

Figure 4: Perspective view of the ACT/FHS's LIDARs field of view at a height of 100 m and the outline (green) of its intersection (footprint) with the ground plane.

The works presented in Refs. [6] and [8] are aiming to achieve full mission planning capabilities with travelled distances significantly exceeding the perception system's detection range. In contrast, the presented work focuses on the final phase only, when the vehicle's distance is approximately two to three times the sensor range from the intended landing location. Furthermore, the LiDAR installed in the ACT/FHS is body-fixed and always facing forward, which limits the benefits of a prior flyover. Given the sensor configuration, the system presented here uses LiDAR

[1] Formerly known as HELLAS-W

data collected during the final approach only, mimicking the final approach reconnaissance type seen in Figure 1 (d.). This may significantly reduce the overall time to landing compared to a mission scenario including a reconnaissance fly-by but urges the need of real-time capable computer-based decision making.

A simplified high-level overview of the system architecture is given in Figure 5. Only relevant parts of the ACT/FHS's complex experimental system are shown for clarity. Modules which record data seen in this work are marked with an asterisk [*].

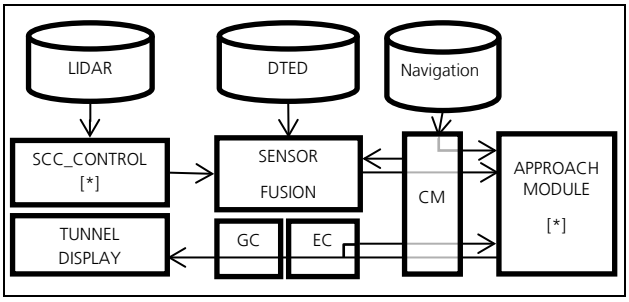

Figure 5: System architecture

A geo-referenced rectangular area of interest is specified to be used in the sensor fusion module[2], which prefills this area with Digital Terrain Elevation Data (DTED) – in the present case data from the Shuttle Radar Topography Mission (SRTM3) with 90 m spacing.

At the start of the intended mission an initial path is calculated. While following this initial path, LiDAR data are continuously combined with DTED to a partial digital surface model (DSM), now including previously unmapped objects on the surface in areas which have been scanned. Since neither the term DEM nor DSM is fully applicable for this combined DEM/DSM, it is referred to as base map (map_b) in the following.

The approach module, being the main focus of this work, is executed as soon as an updated base map by the sensor fusion module is handed over by a communication middleware (CM) and serves two purposes. It handles obstacle events and is responsible for finding a new flight path. In case a solution can be found, it is sent to the experimental computer (EC) which hands it over to a graphics computer (GC) rendering a tunnel-in-the-sky instrument (see Ref. [16]). The following section describes the approach module's internal decision making in more detail.

3. PLANNING

First of all, safety distance calculation and obstacle event handling shall be outlined. A real-world situation which was recorded during a sensor acquisition flight during the project ALLFlight is used as a demonstrational example, see Figure 6.

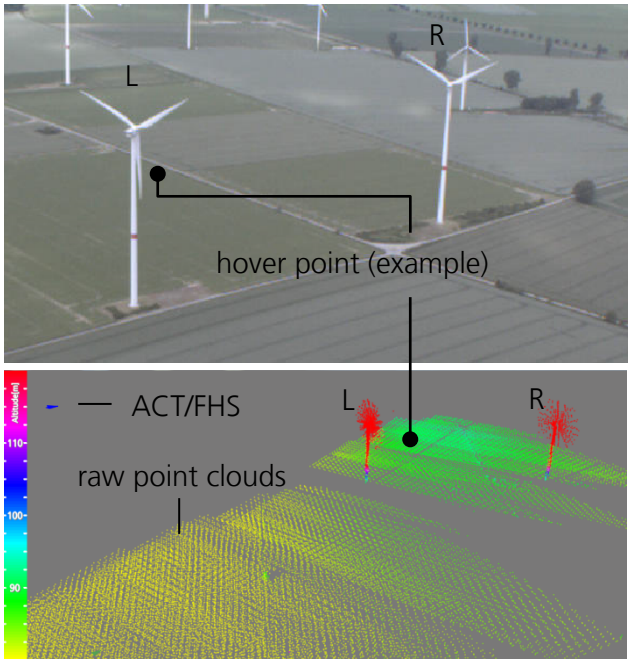

Figure 6: Several wind turbines in an image captured by a forward-facing camera (above) mounted on the ACT/FHS and an exocentric view of corresponding LiDAR point clouds (below) collected over several seconds of flight, created post-flight using *scc_control*.

The upper part of Figure 6 shows a camera image of the ACT/FHS's TV-OUT camera captured in a height above ground level (AGL) of approximately 250 m, showing an exemplary hover point and several previously unmapped wind turbines. The two closest ones are marked with the letters "L" and "R" in the following figures respectively. Due to consecutive scans of the turning turbine blades, these embody rather discs than individual blades in the accumulated point cloud shown in the lower part of Figure 6**.**

3.1. Safety distances

The fused base map, as seen in Figure 7 is determined by the sensor fusion module F3S which registers these raw point clouds onto an equally spaced grid of 5 m spacing, prefilled with DTED data. Since the combined DEM/DSM model contains only one height value per cell, the wind turbines are now transformed into wider, static obstacles spanning the whole rotor width.

In order to ensure clearance to the terrain, a configurable spherical pattern is applied to the neighborhood of each cell of the base map, resulting in a safe map (map_s). Figure 7 depicts both, the base and safe maps of the surrounding area of the wind turbines seen in Figure 6.

[2] Here: Flexible Sensor Simulation Suite (F3S), see Ref. [15]

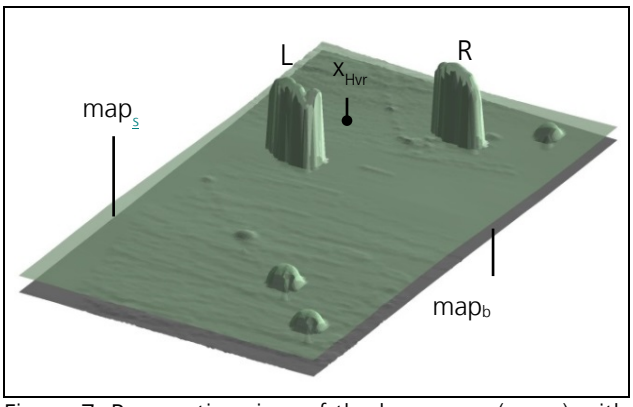

Figure 7: Perspective view of the base map (map_b) with added safety distances (map_s)

The transparent surface over the base map illustrates the resulting safe map with an added safety distance of two rotor diameters (20 m). An active path is declared as unsafe, as soon as it penetrates the safe map, resulting in an obstacle event and the execution of a re-planning.

3.2. Visibility hull based planning

When trying to reach a landing point in an unmapped three-dimensional environment, collecting the highest amount of (visual) information is highly prioritized by pilots. The following first three instructions from the double angle approach procedure from Ref. [4] clearly emphasize this statement.

- "Initially a shallow angle may be flown to a point on the other side of the landing site until the landing area is visible"
- "Once the touchdown point is visible, the angle is steepened for final approach to hover"
- "Hold line of sight with small corrective movements"

Related visibility problems are widely studied, but either restricted to polygonal shapes in 2D [17,18] or used in computer graphics applications using triangles as geometric primitives, none of which natively applies to our world model. The key idea of the presented path planning strategy is derived from the procedure mentioned above and Refs. [19] and [20].

In Ref. [19], virtual cameras are moved in 3D space while considering longest visibility of an object of interest (focus) along the way. Moreover, the work on visibility path planning in Ref. [20] was found to be a valuable resource for the given problem as well. Therein, path optimization criteria include best surveillance of an area which in contrast allows stealth operations. Their proposed concept of so called visibility hulls is used as intermediate data structure for line-of-sight queries in 3D space. An overview of the developed path re-planning strategy is given in Figure 8 by using a two-dimensional example for illustrational purposes.

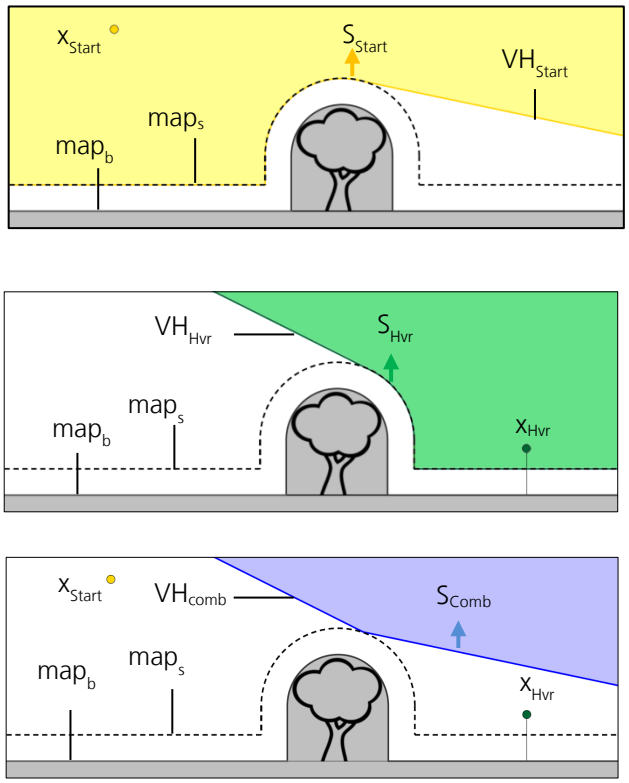

Figure 8: Combined Visibility Hull (VH) concept (2D)

Consider the situation depicted in the upper third of Figure 8, showing a single obstacle and the corresponding base and safe maps. The free space above the dotted line has ensured obstacle clearance to the map below.

Given a surface of reference and an observer point, the visibility hull from Ref. [20] divides the space above it into two subsets. All points above it do have a direct line of sight to the observer point, the points below do not. In the two upper thirds of Figure 8, the yellow and green lines depict the visibility hulls $VH_{Start/Hvr}$ corresponding to their respective observer points $x_{Start/Hvr}$) in the same color, applied to a safe map. Let now S_{Start} and S_{Hvr} be the point sets in space above the visibility hulls of x_{Hvr} and x_{Start} respectively, indicated with an arrow and marked as filled areas in Figure 8.

The intersection $S_{comb}=S_{Hvr} \cap S_{Start}$ as seen in the lower part of Figure 8 contains the subset of space which has a direct connection to both of these points. One can observe that the lower bound of this subset is the higher of both visibility hulls. The resulting separating object, a line in the 2D case in the lower part of Figure 8, is referred to as combined visibility hull VH_{comb} in the following. Transferring this concept to the third spatial dimension, all visibility hulls transform to surfaces instead of lines. An example using the real terrain already seen in Figure 6 is shown in Figure 7 for comparison.

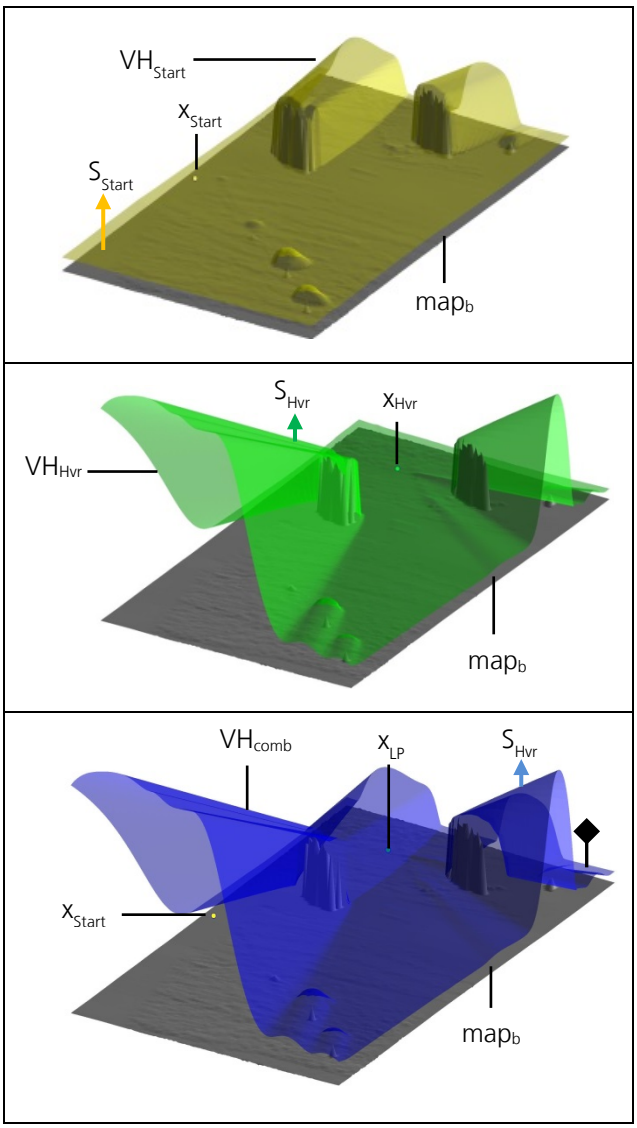

Figure 9: Combined Visibility Hull concept (3D)

Note that only the visibility hulls are drawn in 3D, the corresponding sets S_{Start}, S_{Hvr} and S_{comb} are the spaces above these surfaces respectively, only indicated by arrows to avoid cluttering.

Each point lying in the space above VH_{comb} has a direct connection to the intended hover point, the predicted vehicle position and at least minimal obstacle clearance. These points are therefore basically candidates for a two-segment path from x_{Start} to x_{Hvr}, similar to the double angle approach procedure described earlier. Now consider a point at the black diamond symbol in the lower third of Figure 9, which is to the right of the right wind turbine in Figure 6. Since it is above the combined visibility hull, a two segment path from X_{Start} to X_{Hvr} would be free to pass, but it is unlikely that a pilot would choose such a detour. This raises the question, how the decision making process in such a situation can be modelled systematically.

3.3. Flight path rating

After the combined visibility hull is calculated, candidate points above it are sampled for further evaluation. Depending on the intended outcome, which may e.g. be a restriction to vertical avoidance only, these candidate points may be sampled in a specific plane or volume in space.

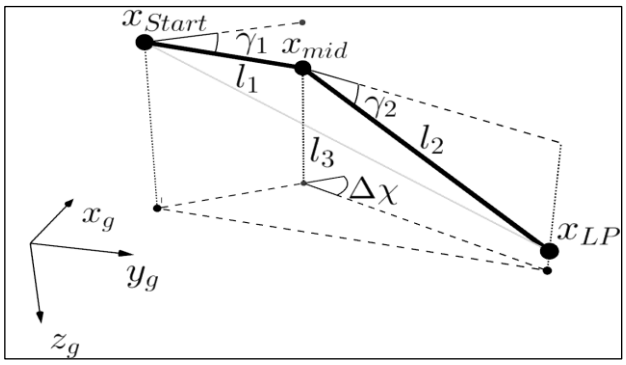

Figure 10: geometric parameters used for path evaluation

The parameters depicted in Figure 10 and the overall length $l_{Sum}=l_1+l_2$ are now used for evaluation of the heuristic object function (rating) given in Equation 1, which is designed to prioritize solutions with higher pilot acceptance.

$$r(x_{mid}) = \prod_{1\le i\le n} h_i \prod_{1\le j\le m} s_j \tag{1}$$

The function includes two types of criteria, namely hard (h_i) and soft (s_j) ratings. The prior are handled like boolean expressions (0 or 1) to exclude inacceptable solutions early in the process and the equations for the latter are designed to express different motivations ($0 \le r(x_{mid}) \le 1$). The following Table 1 summarized three hard and two soft criteria to be used for the rating function.

Motivation	**Equation**
Small track angle changes	$h_1 = \begin{cases} 1, & if\ \lvert\Delta\chi\rvert > \Delta\chi_{max} \\ 0, & otherwise \end{cases}$
No ascending first segment	$h_2 = \begin{cases} 1, & if\ \gamma_1 > 0 \\ 0, & otherwise \end{cases}$
Steeper second segment	$h_3 = \begin{cases} 1, & if\ \gamma_1 > \gamma_2 \\ 0, & otherwise \end{cases}$
Straightness	$s_1 = \frac{l_3}{l_{sum}}$
Long second (final) segment	$s_2 = \frac{l_2}{l_{sum}}$

Table 1: hard and soft criteria influencing the choice of an avoidance path

Note that small track angle changes (h_1) and a steeper second segment (h_3) only apply as criteria in the three-dimensional case and when lateral maneuvers are considered. A long second segment (s_2) is the main driver of assuring a long time of visual contact to the intended landing location. Summarized, the proposed procedure of finding a two-segment solution from a startpoint x_{start} to the goal x_{Hvr} now uses the following five steps:

1) Calculate $VH_{Hvr}(map_{safe}, x_{Hvr})$.
2) Calculate $VH_{Start}(map_{safe}, x_{Start})$.
3) Calculate $VH_{comb} = \max(VH_{Start}, VH_{LP})$
4) Select candidate points above VH_{comb}.
5) Evaluate candidate points.

The solution with the highest rating is selected, smoothed and a velocity profile with constant deceleration is applied. In case no solution exists, the algorithm reports failure.

4. FLIGHT TRIAL

During previous flight trials in 2013 [11], a shallow approach to a spot on the taxiway at Braunschweig airport was chosen as a test scenario for the toolchain of in-flight LiDAR acquisition, sensor fusion and path planning. A map view from Openstreetmap[3] can be seen in Figure 11.

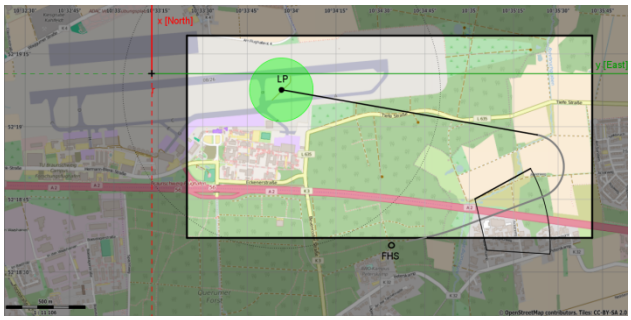

Figure 11: Landing point and approach direction at Braunschweig airport

In the above figure, a top view of the area with the highlighted area used for LiDAR data accumulation by the sensor fusion module (F3S) is shown. The local geodetic frame used for referencing the map is located in the upper left quadrant of the figure.

4.1. Preparation

Before being released for the flight trial, the presented planning strategy was extensively tested in a desktop environment using data recorded during the 2013 flight trails. Additionally, closed-loop simulations in the air vehicle simulator (AVES), [21] were carried out. AVES is DLR's flight simulation facility in Braunschweig, used for system development and flight test preparation. It contains a complete replication of the ACT/FHS' cockpit and experimental system including LiDAR sensor simulation in virtual environments [15] like the airport area as seen in Figure 11.

4.2. Execution

On May 11th in 2015, an experienced evaluation pilot (EP) holding a test pilot license was conducting approaches to the landing location. The given task was to follow the tunnel gates of 60 m width and 40 m height in the instrument as seen in the left of Figure 12. Starting with an initial true air speed (TAS) between 50 and 60 kts, a hover state 30 ft above the intended taxiway location should be reached. The EP had previously taken part in several flights using the tunnel-in-the-sky display seen in Figure 12 and was therefore already familiar with the instrument.

Figure 12: Evaluation pilot (EP) during the trial following the flight path with a Tunnel-in-the-sky instrument and flight test engineer workstation

The flight test engineer (FTE) located in the back of the ACT/FHS observed several relevant system states. The FTE observed the state of the current base map on a moving map display in a color-coded representation and verbally communicated replanning events to the evaluation pilot during flight.

4.3. Results

Overall five approaches were flown during the flight trial. An overview of raw LiDAR data collected during the third approach is shown in Figure 13 from a north-facing perspective, with three emphasized positions marked with A, B and C. Figure 14 shows camera and LiDAR snapshots for these three positions.

Comparing the top view in Figure 11 and the point cloud in Figure 13, the motorway, an inhabited area and the trees in the final approach can be seen. Large and small scale details like the fence in the left part of the LiDAR image at position C in Figure 13 indicate the captured detail of the scene and were mapped into the base map in a lower resolution grid of 5 m

[3] http://www.openstreetmap.org

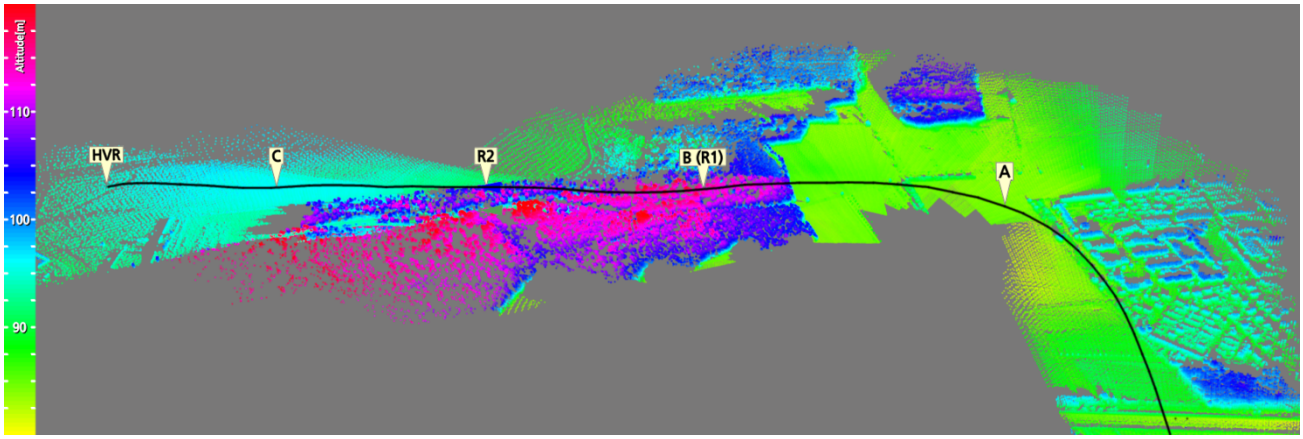

Figure 13: Post-processed exocentric view of accumulated high density LiDAR point clouds, recorded by *scc_control* and color-coded with respect to mean sea level (MSL). The hover point (HVR) and two positions of trajectory changes (R1, R2) are marked along the flight path (black line). The helicopters position is approximately at R2.

spacing which was used for planning.

During this approach, the trajectory was changed two times at positions marked with R1 and B(R2) in Figure 13.

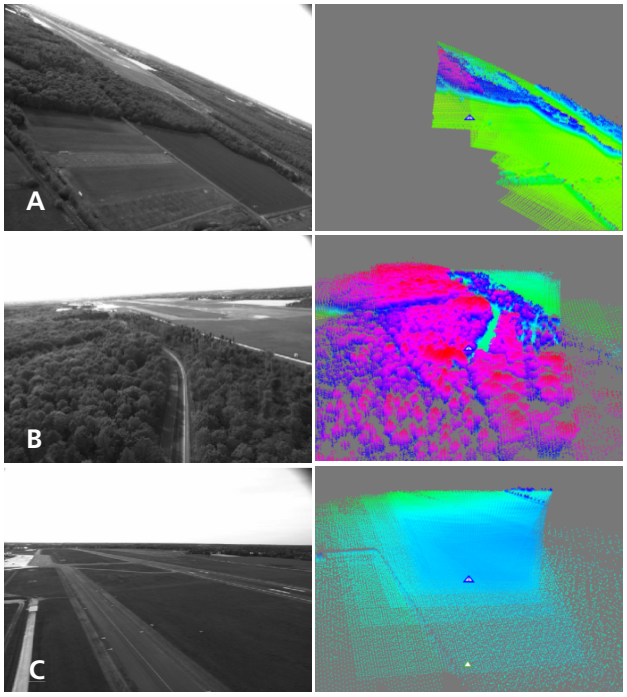

Figure 14: Camera (left) and LiDAR data (right) at three positions (A,B,C) during 3rd flown approach. The triangular symbol in the center of the LiDAR pictures indicates the ACT/FHS's position. See Figure 13 for LiDAR color scale.

In Figure 15, the approach module results for the first trajectory change at position B (R1) in this approach are shown. The red X indicates a penetration of the active path (black) with the safe map. The noisy area above it, indicated by a white arrow, is a typical problem which may occur when actual sensor data is merged with a-priori data in digital surface models, resulting in these high frequency ("spiky") areas. Such spikes might as well occur around the landing spot when the coverage of its surrounding is irregular.

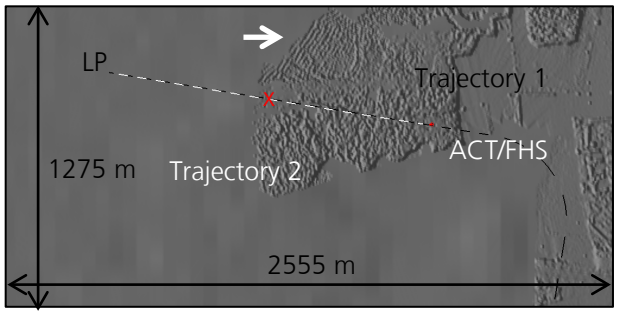

Figure 15: base map at position of first replan B (R1) in third approach

The perspective view in the upper part of Figure 16 shows the overlaid safe map mentioned earlier, the active path (black) and the corrected path (white) after the trees were detected. The enlarged images taken from the cockpit camera in the lower part of Figure 16 indicate the trajectory change as a slight upward displacement as seen by the pilot. Similar trajectory changes occurred during all of the mentioned runs, in some cases nearly unnoticed by the evaluation pilot who was focusing his attention on the given task of path following.

Although the obstacles and approach direction did not change, the number of trajectory changes per approach varies due to slightly different sensor coverage and runtime behavior, see Table 2.

Approach Number	1	2	3	4	5
Trajectory changes	1	3	2	1	2

Table 2: Trajectory changes during the five approach

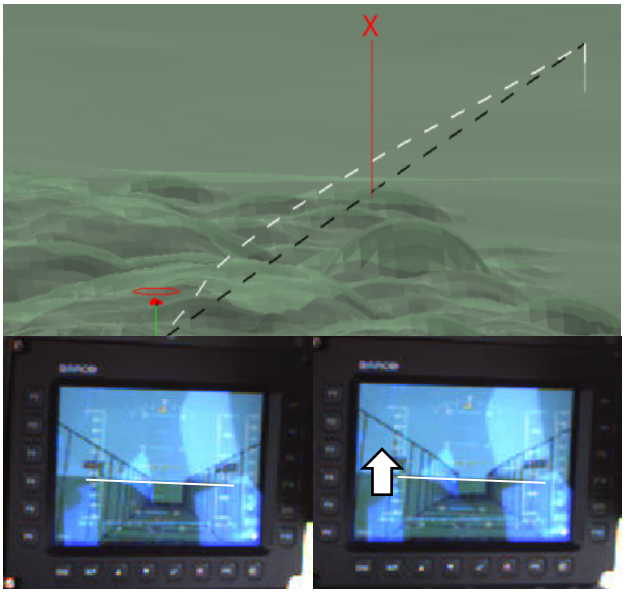

Figure 16: First trajectory change during third approach, showing a perspective view in the upper part including the safe map and active (black) and newly calculated (white) flight paths. The corresponding switch in the tunnel display is shown below.

An analysis of the lateral and vertical deviation of the flight paths to the tunnel's center during the final straight path of the flight is shown in Figure 17 for the sake of completeness. The absolute deviation was not exceeding 20 m during most of the flight. However, workload or path following performance is beyond the scope of this work and needs to be addressed in further studies with more participants.

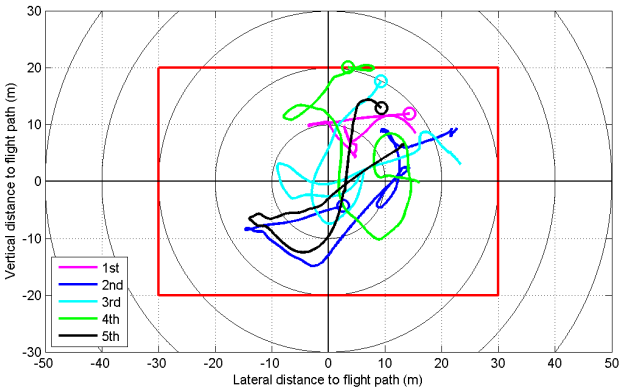

Figure 17: Lateral and vertical deviation during the final, straight part of the five flown approaches. The circular marker indicates the deviation at start

The processing times[4] of the approach module including the presented visibility hull strategy never exceeded two seconds on the target system (1.4 Ghz Pentium M, 2 GB RAM). In contrast to the 2013 trial, no too frequent re-planning or gaps between the trajectories were reported by the evaluation pilot this time. Representing of the map the map in a color-coded representation was rated as very helpful by the flight test engineer.

[4] Including input cross-checks, planning and file operations for plot data of approximately 1.4 MB file size

5. CONCLUSION AND OUTLOOK

In this work, a fast and robust method of approach trajectory calculation is described, applicable for helicopter landing. The results demonstrate that the proposed system is able to react immediately under real-world conditions to potential obstacles in a previously unmapped environment, showing appropriate reactions in all of the five approaches. In order to realize safer landings on unprepared sites for helicopters, an enhanced planning strategy for the final approach is presented continuing research efforts undertaken in recent years in that field [5, 11].

While the used head-down tunnel display allows the pilot to follow a geo-referenced flight path with certain accuracy, it is not optimized to communicate the current state of system perception or planning decisions to the pilot - a crucial point in pilot's system acceptance.

However, an alternative human-machine interface using a helmet-mounted-display is already part of an adjacent study in cooperation with Airbus DS Electronics and Border Security GmbH [22]**,** addressing the above mentioned points using state-of-the-art 3D symbols, rendered conformal to the pilot's outside view.

ACKNOWLEDGEMENT

The author likes to thank the colleagues in our flight controls group for their support during the trial Moreover, the colleagues at the Institute of Flight Guidance are greatly acknowledged for their continuous help with LiDAR related issues. Special thanks to Johannes Wartmann for providing MATLAB tools used in the path deviation analysis.

References

AHS = American Helicopter Society

AHSF = American Helicopter Society Forum

[1] Hörhager, "Oben blau, unten grau", 1414 – Das Magazin der REGA, May, 2015, www.rega.ch

[2] Bernandersson, "Analysis of 2006-2010 European Helicopter Accidents - Final EHSAT Analysis Report", European Helicopter Safety Team, 2015

[3] Anon., "The Compendium Report: The US JHSAT Baseline of Helicopter Accident Analysis, Volume II, (CY2000, CY2001, CY2006)," US Joint Helicopter Safety Analysis Team, July, 2011

[4] Anon., OFF Airfield landing site operations – Methods to improve Helicopter pilots safety. Training leaflet, EHEST, 2012

[5] Lantzsch, R., Greiser, S., Wolfram, J., Wartmann, J., Müllhäuser, M., Lüken, T., Döhler, H.-U., and Peinecke, N., "ALLFLIGHT: Helicopter pilot assistance in all phases of flight," 68th AHSF, Fort Worth, TX, May 1-3, 2012

[6] Whalley, M. S., Takahashi, M. D., Fletcher, J. W., Moralez, E., Ott, C., Olmstead, M. G., Goerzen, C. L., Schulein, G. J., Savage, J. C., Burns, H. N., and Conrad, B., "Flight Test Results for Autonomous Obstacle Field Navigation and Landing Site Selection on the RASCAL JUH-60A," 69th AHSF, Phoenix, AZ, USA, May 21-23, 2013

[7] Mettler, B., Kong, Z., Goerzen, C., and Whalley, M., "Benchmarking of Obstacle Field Navigation Algorithms for Autonomous Helicopters," 66th AHSF, Phoenix, AZ, USA, May 11-13, 2010.

[8] Chamberlain, L., Scherer, S., and Singh, S., "Self-Aware Helicopters: Full-Scale Automated Landing and Obstacle Avoidance in Unmapped Environments," 67th AHSF, Virginia Beach, VA, USA, May 3-5, 2011

[9] Münsterer, T., Völschow, P., Singer, B., Strobel, M. and Kramper, P., "DVE flight test results of a sensor enhanced 3D conformal pilot support system," *Proc. SPIE* 9471, Degraded Visual Environments: Enhanced, Synthetic, and External Vision Solutions 2015, 947106 Baltimore,MD, USA June 11, 2015; doi:10.1117/12.2180634;

[10] Szoboszlay, Z. P., Fujizawa, B. T., Ott, C. R., Savage, J. C., Goodrich, S. M., McKinley, R. A., and Soukup, J. R., "3D-LZ Flight Test of 2013: Landing an EH-60 L Helicopter in a Brownout Degraded Visual Environment," 70th AHSF, Montréal, Québec, Canada, May 20-22, 2014

[11] Zimmermann, M., König, C. "Integration of a visibility graph based path planning method in the ACT/FHS rotorcraft", CEAS Aeronautical Journal, 7(3), 391-403

[12] Strohmaier, T., "Computerbasierte Trajektorien-generierung für einen bemannten Hubschrauber auf einen unvorbereiteten Landeplatz," PhD Thesis, TU Braunschweig, 2010

[13] Lüken, T., Peinecke, N., Schmerwitz, S., and Doehler, H.-U., "ALLFlight - Helicopter Flight Trials under DVE conditions with an AI-130 mmW radar system," 37th European Rotorcraft Forum, Southampton, United Kingdom, September 13-15, 2011

[14] Schulz, K.R., Scherbarth, S., Fabry, U., „Hellas, Obstacle warning system for helicopters", Proceedings of SPIE, Vol 3723, pp. 1-8 (2002)

[15] Peinecke, N., Döhler H.-U. and Korn, B.R., „Simulation of Imaging Radar Using Graphics Hardware Acceleration", Proc. SPIE, Enhanced and Synthetic Vision, Vol 6957, pp. 695-720, Orlando, FL, March 17-20, 2008

[16] Gursky, B., Olsman, W., and Peinecke, N., "Development of a tunnel-in-the-sky display for helicopter noise abatement procedures," CEAS Aeronautical Journal, Vol. 5, No. 2, 2014, pp. 199–208.

[17] Ghosh, S.K., "Visibiliy Algorithms in the Plane", Cambridge University Press, 2007

[18] Obermeyer, K. J. and Contributors, "The VisiLibity library," http://www.VisiLibity.org, 2008, R-1.

[19] Oskam, T., Sumner, R. W., Thuerey, N., and Gross, M., "Visibility transition planning for dynamic camera control," 2009 ACM SIGGRAPH/ Eurographics Symposium on Computer Animation - SCA '09, Vol. 1, 2009, pp. 47-57.

[20] Srikanth, M. B., Mathias, P. C., Natarajan, V., Naidu, P., and Poston, T., "Visibility volumes for interactive path optimization," The Visual Computer, Vol. 24, No. 7-9, 2008, pp. 635–647

[21] Duda, H., Gerlach, T., Advani, S., and Potter, M., "Design of the DLR AVES Research Flight Simulator,"AIAA Modelling and Simulation Technologies Conference (MST), Boston, MA, USA Aug. 19-22, 2013

[22] Wolfram, J., Zimmermann, M., Klasen, S., Gestwa, M., „Design of an automatic Transition to Hover system", German Aerospace Congress, Braunschweig, Sept. 13-15, 2016